Application of SMES to Enhance the Dynamic Performance of DFIG During Voltage Sag and Swell

A. M. Shiddiq Yunus, *Student Member, IEEE*, Mohammad A. S. Masoum, *Senior Member, IEEE*, and A. Abu-Siada, *Member, IEEE*

Abstract—**The integration of wind turbines into modern power grids has significantly increased during the last decade. Wind turbines equipped with doubly fed induction generators (DFIGs) have been dominating wind power installation worldwide since 2002. In this paper, a superconducting magnetic energy storage (SMES) unit is proposed to improve the dynamic performance of a wind energy conversion system equipped with DFIG during voltage sag and voltage swell events. The converter and the chopper of the SMES unit are controlled using a hysteresis current controller and a fuzzy logic controller, respectively. Detailed simulation is carried out using MATLAB/SIMULINK software to highlight the impact of the SMES unit in improving the overall system performance under voltage sag and voltage swell conditions.**

Index Terms—**Doubly fed induction generator (DFIG), fuzzy logic, hysteresis current controller (HCC), superconducting magnetic energy storage (SMES), voltage sag, voltage swell and wind energy conversion system (WECS).**

I. INTRODUCTION

UTILIZATION of renewable energy sources is becoming more attractive due to the detrimental impact of conventional energy resources on the environment. Implementation of carbon tax in some countries has also been considered as a trigger to accelerate the utilization of renewable energy sources [1]. One of the most promising renewable energy sources is wind energy, which has grown rapidly from about 2000 MW at the end of the year 1990 to 94000 MW by the end of the year 2007. The future prospects of the global wind industry are very encouraging, and it is estimated to grow by more than 70% to reach 160 GW by the year 2012. It is estimated that, by the year 2020, wind power will supply at least 10% of global electricity demands [2]. Owing to the rapid development of power electronics technology, the number of wind turbines

equipped with converter stations has increased. The doubly fed induction generator (DFIG) is one of the most popular variable-speed wind turbine generators (WTGs). In this technology, the rotor winding is connected to a coupling transformer through a back-to-back partial-scale voltage source converter (VSC), whereas the stator winding is directly connected to the grid at a point of common coupling (PCC) through the coupling transformer. The VSC decouples the mechanical and electrical frequencies and make variable-speed operation possible [3]. Global trend shows that the market share of the installed wind energy conversion system (WECS) has been dominated by DFIG-based wind turbines since 2002 [4]. In the earlier stages of integrating WECSs into the electricity grids, WTGs were disconnected from the grid during faults at the grid side to avoid any possible damages to wind turbines. Recently, existing WTGs, however, will have to be designed/managed to comply with the recent requirements of new grid codes [5] to assure the continuity of supplying power to the grid during transient and abnormal operating conditions. There are two strategies that can be applied to improve the performance or the fault ride through (FRT) capability of the DFIG. First is by developing new control techniques to fulfill the criterion of the transmission system operators, as presented in most of the literature [6]–[10]. However, this strategy is effective for new installation and new connection of WECSs to the grid. Second is by applying FACTS devices or storage energy systems [11], which are a more cost effective choice for existing WECSs. Variable-speed WECSs such as DFIG were introduced to overcome the weakness of the fixed-speed type in capturing maximum wind energy and to contribute in supplying reactive power to the grid when required [12]. Compared with full-scale variable-speed WECSs, DFIG is very sensitive to grid faults [7], where, even though the DFIGs are connected far away from the grid, the grid faults will influence the voltage profile at the PCC. Moreover, during grid fault, voltage drop at the DFIG terminal, high current flow at both grid and rotor side converters, and high voltage across the dc link capacitor may lead to converter station blocking. This condition will be ended by the disconnection of the DFIG from the system. If the DFIG contributes in delivering a large portion of power to the grid, financial loss will be uncountable. Most of the studies about the DFIG are concerned about the improvement of its FRT capability during voltage sag [6]–[10]. No attention however is given to improve the DFIG performance under voltage sag and voltage swell

This article has been accepted for inclusion in a future issue of this journal. Content is final as presented, with the exception of pagination.

2   IEEE TRANSACTIONS ON APPLIED SUPERCONDUCTIVITY
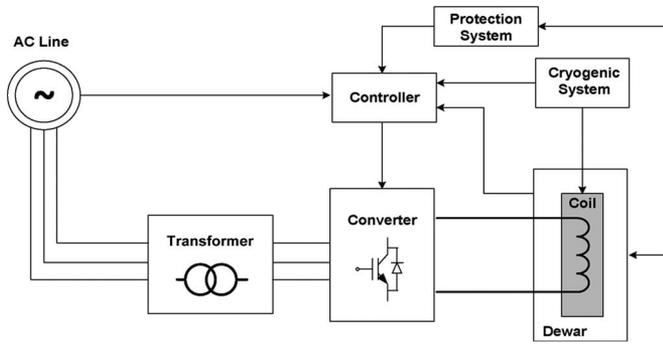

Fig. 1.   Typical schematic diagram of an SMES unit.

conditions using the same controller. Although the swell event in the grid side is rarely to occur, it can cause voltage rise at the PCC that may violate the grid codes' requirements. Recently, the maximum voltage ride through of Spain [13] and Australia's [14] grid codes is set to 1.3 pu. If the voltage profile at the PCC rises above 1.3 pu, the WTGs have to be disconnected from the grid.

Since the successful installation of the 30-MJ superconducting magnetic energy storage (SMES) unit at Bonneville power administration, Tacoma, in 1982 [15], SMES has attracted many researchers to study its potential applications in power systems [16]–[18]. There are many papers in the literature that investigated the application of SMES to WECSs. However, most of these studies have only focused on the use of the SMES unit to smooth the output power of fixed-speed WECSs during wind speed fluctuation to avoid system instability [19]–[26].

This paper presents a new application of the SMES unit to improve the performance of a wind turbine equipped with DFIG during voltage sag and voltage swell at the grid side. A new control system for the SMES unit based on hysteresis current control in conjunction with fuzzy logic control is proposed. The Simulink/Matlab software is used to simulate the wind turbine, the SMES unit, and the model under study. Results are analyzed to highlight the improved dynamic performance of WECSs in conjunction with the SMES unit.

II. SMES

An SMES system consists of a superconductor coil, a power-conditioning system, a cryogenic refrigerator, and a cryostat/vacuum vessel to keep the coil at a low temperature required to maintain it in superconducting state.

This configuration makes SMES highly efficient in storing electricity with typical efficiency in the range of 95%–98% [27]–[29]. Other advantages of the SMES unit include very quick response and possibilities for high-power applications [30]. A typical SMES configuration is shown in Fig. 1.

III. SYSTEM UNDER STUDY

The system under study shown in Fig. 2(a) consists of six 1.5-MW DFIGs connected to the ac grid at the PCC. The DFIG consists of an induction generator with stator winding connected directly to the grid through a Y/Δ step-up transformer, whereas the rotor winding is connected to a bidirectional
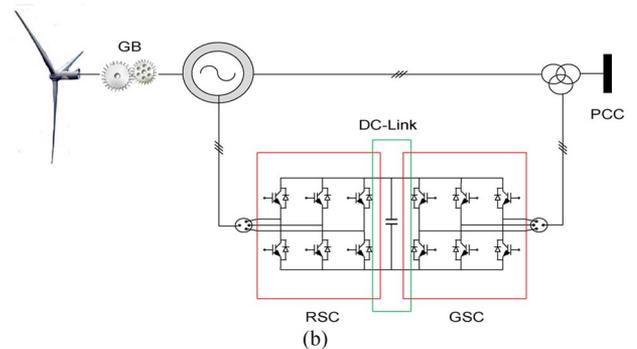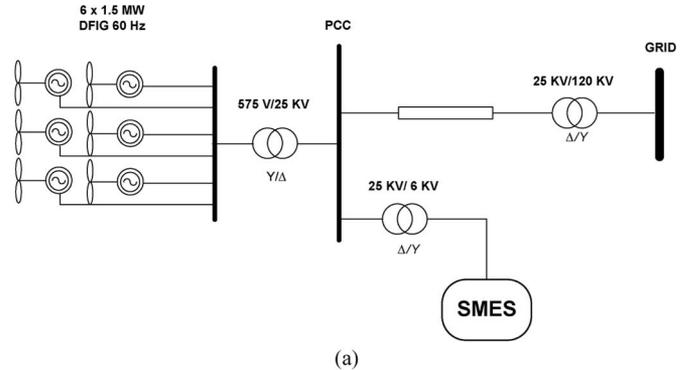

Fig. 2.   (a) System under study. (b) Typical configuration of an individual DFIG.

TABLE I
PARAMETERS OF THE DFIG

Duty Cycle (D)	SMES Coil Action
$D = 0.5$	standby condition
$0 \le D < 0.5$	discharging condition
$0.5 < D \le 1$	charging condition

TABLE II
PARAMETERS OF THE TRANSMISSION LINE

Rated Power	9 MW (6 x @ 1.5 MW)
Stator Voltage	575 V
Frequency	60 Hz
R_S	0.023 pu
R_R	0.016 pu
V_{DC}	1150 V

back-to-back insulated gate bipolar transistor (IGBT) VSC, as shown in Fig. 2(b). The grid that is represented by an ideal three-phase voltage source of constant frequency is connected to the wind turbines via a 30-km transmission line and Δ/Y step-up transformer. The reactive power produced by the wind turbines is regulated at zero MVar under normal operating conditions. For an average wind speed of 15 m/s, which is used in this study, the turbine output power is 1.0 pu, and the generator speed is 1.2 pu. The SMES unit is connected to the 25-kV bus and is assumed to be fully charged at its maximum capacity of 1.0 MJ Tables I and II.

IV. SMES CONTROL APPROACHES

Generally, there are two major configurations of SMES, i.e., current source converter (CSC) and VSC. Traditionally, CSC is

This article has been accepted for inclusion in a future issue of this journal. Content is final as presented, with the exception of pagination.

YUNUS *et al.*: APPLICATION OF SMES TO ENHANCE PERFORMANCE OF DFIG DURING VOLTAGE SAG AND SWELL 3
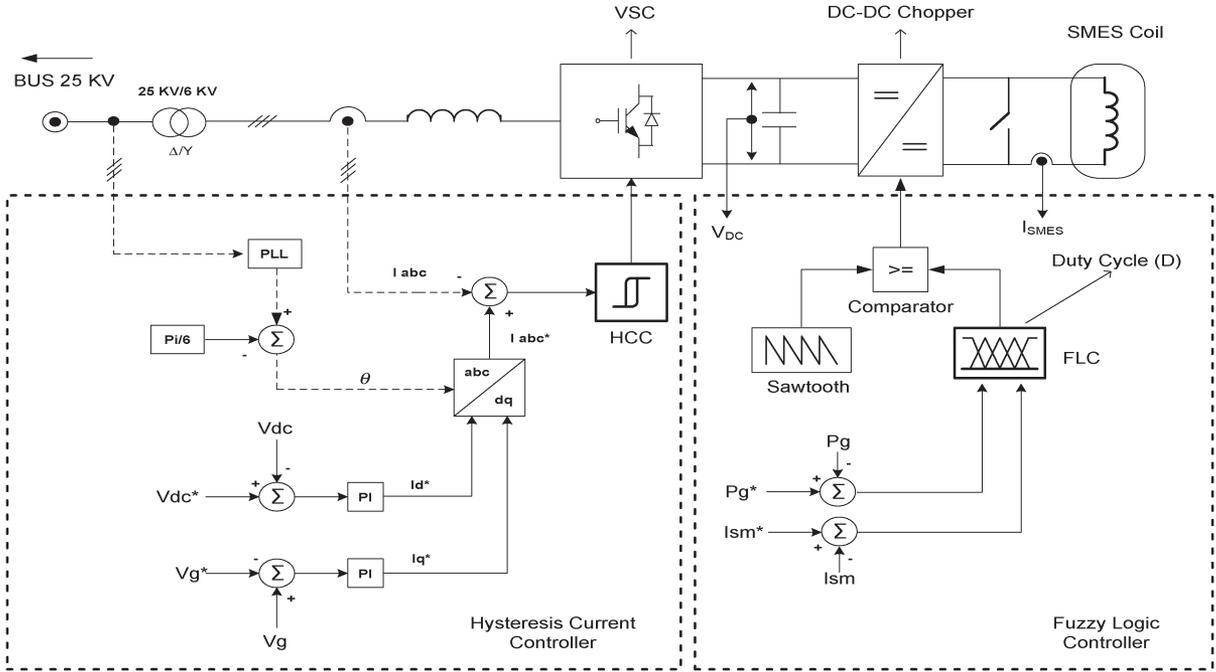

Fig. 3. SMES unit configuration and the proposed HCC–FLC control scheme.

connected through a 12-pulse converter configuration to eliminate the ac-side fifth and seventh harmonic currents and the dc-side sixth harmonic voltage, thus resulting in significant savings in harmonic filters [18]. However, because this configuration uses two 6-pulse CSCs that are connected in parallel, its cost is relatively high. The VSC, on the other hand, must be connected with a dc–dc chopper through a dc link, which facilitates energy exchange between the SMES coil and the ac grid. Reference [31] estimates the total cost of the switching devices of the CSC to be 173% of the switching devices and power diodes required for equivalent capacity of the VSC and the chopper. Moreover, a VSC has a better self-commutating capability, and it injects lower harmonic currents into the ac grid than a comparable CSC. The use of IGBTs in this configuration is more beneficial than GTO since the switching frequency of an IGBT lies on the range of 2–20 kHz, whereas, in case of GTO, the switching frequency cannot exceed 1 kHz [4].

The proposed SMES configuration used in this paper consists of a VSC and dc–dc chopper, as shown in Fig. 3. The converter and the chopper are controlled using a hysteresis current controller (HCC) and a fuzzy logic controller (FLC), respectively. The stored energy in the SMES coil can be calculated as

$$E = \frac{1}{2} I_{\mathrm{SMES}}^2 L_{\mathrm{SMES}} \qquad (1)$$

where E, I_{SMES}, and L_{SMES} are the stored energy, current, and coil inductance of the SMES unit, respectively.

While the control system of the dc–dc chopper is presented in [32], the control approach for the VSC as part of the SMES configuration is not presented. In contrast with [32], the dc–dc chopper control system is not presented in [19]. The configuration of SMES in [33] is new, but its application is limited for low WTG capacity, and since the SMES coil is proposed to be connected to the individual DFIG's converters, this topology will

be only appropriate for new WECS installations. Application of the SMES system to microgrids is presented in [34], where the SMES is used to stabilize the entire microgrid system. The control scheme presented in this work is very complex because it is working for three different levels of controls; this will lead to high implementation and maintenance cost. Moreover, it requires a robust computational system.

The proposed control algorithm in this paper is much simpler and closer to realistic applications, compared with the similar controller proposed in [16] and [21]. In the aforementioned papers, four proportional–integral (PI) controllers are proposed, which require more computational time to optimally tune its parameters to maintain overall system stability and to achieve satisfactory dynamic response during transient events. Moreover, the control system for the dc–dc chopper in these studies considered only the DFIG-generated active power (P_G) as a control parameter, but it ignored the energy capacity of the SMES unit. The control scheme in this paper comprises only two PI controllers and considers the SMES coil current to take the SMES stored energy capacity into account, along with the DFIG generated power as control parameters to determine the direction and level of power exchange between the SMES coil and the ac system. This control system is efficient, simple, and easy to implement, as will be elaborated here.

A. HCC

The HCC is widely used because of its simplicity, insensitivity to load parameter variations, fast dynamic response, and inherent maximum-current-limiting characteristic [35]. The basic implementation of the HCC is based on deriving the switching signals from the comparison of the actual phase current with a fixed tolerance band around the reference current associated with that phase. However, this type of band control
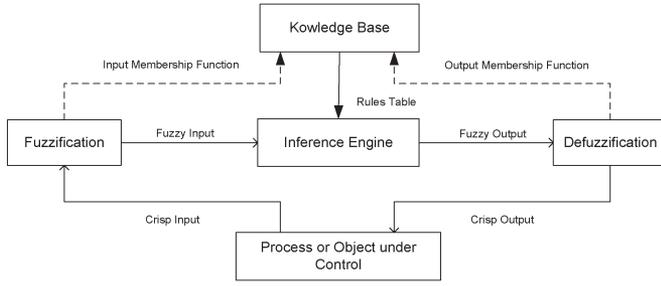
This article has been accepted for inclusion in a future issue of this journal. Content is final as presented, with the exception of pagination.

4   IEEE TRANSACTIONS ON APPLIED SUPERCONDUCTIVITY

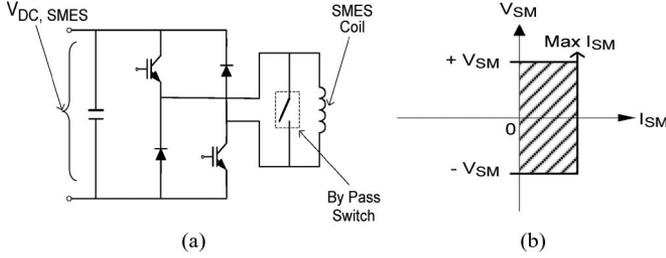Fig. 4.   Structure of the proposed fuzzy controller.

Fig. 5.   (a) Class-D dc–dc chopper topology with an SMES coil. (b) Operation range of the SMES coil.

is not only depending on the corresponding phase voltage but is also affected by the voltage of the other two phases [36]. The effect of interference between phases (referred to as inter-phase dependence) can lead to high switching frequencies. To maintain the advantages of the hysteresis methods, this phase dependence can be minimized by using the phase-locked loop (PLL) technique to maintain the converter switching at a fixed predetermined frequency level [37]. The proposed SMES with an auxiliary PLL controller is shown in Fig. 3. The HCC is com-paring the three-phase line currents (I_{abc}) with the reference currents (I_{abc}^*), which is dictated by the I_d^* and I_q^* references. The values of I_d^* and I_q^* are generated through conventional PI controllers based on the error values of V_{dc} and V_s. The value of I_d^* and I_q^* is converted through Park transformation $(dq0 - abc)$ to produce the reference current (I_{abc}^*).

B. FLC

To control power transfer between the SMES coil and the ac system, a dc–dc chopper is used, and fuzzy logic is selected to control its duty cycle (D), as shown in Fig. 3. The FLC is developed according to the fuzzy inference flowchart shown in Fig. 4, which is a process of formulating the mapping from a given input to the designated output. Input variables for the model are the real power generated by the DFIG and the SMES coil current.

The output of the FLC is the duty cycle (D) for a class-D dc–dc chopper that is shown in Fig. 5(a). The $V–I$ operational range for the SMES coil is shown in Fig 5(b). The duty cycle determines the direction and the magnitude of the power ex-change between the SMES coil and the ac system, as presented in Table III.

If the duty cycle (D) is equal to 0.5, no action will be taken by the coil, and the system is under normal operating condi-tions. Under this condition, a bypass switch that is installed

R_1, R_0 (Ω/km)	0.1153, 0.413
L_1, L_0 (H/km)	1.05×10^{-3}, 3.32×10^{-3}
C_1, C_0 (F/km)	11.33×10^{-9}, 5.01×10^{-9}
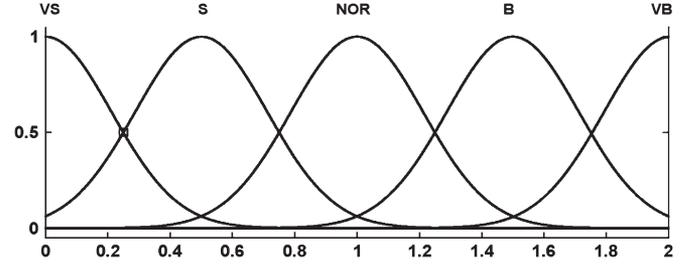
Fig. 6.   MF for the input variable P_G (pu).

across the SMES coil [shown in Fig. 5(a)] will be closed to avoid the draining process of SMES energy during normal operating conditions. The bypass switch is controlled in such a way that it will be closed if D is equal to 0.5; otherwise, it will be opened. This technique has been introduced in some studies in the literature [21], [31]. When the grid power is reduced, D will be reduced accordingly to be in the range of 0–0.5, and the stored energy in the SMES coil will be transferred to the ac system. The charging process of the SMES coil takes place when D is in the range of 0.5–1.

The relation between V_{SMES} and $V_{DC,SMES}$ can be written as [31]

$$V_{SMES} = (1 - 2D)V_{DC,SMES} \qquad (2)$$

where V_{SMES} is the average voltage across the SMES coil, D is duty cycle, and $V_{DC,SMES}$ is the average voltage across the dc-link capacitor of the SMES configuration.

The model is built up using the graphical user interface tool provided by MATLAB. Each input was fuzzified into five sets of Gaussmf-type membership function (MF). The Gaussian curve is a function of a vector x and depends on parameters σ and c, as given by

$$f(x; \sigma, c) = e^{-(x-c)^2/2\sigma^2} \qquad (3)$$

where σ and c are the variables that determine the center of the peak and the width of the bell curve, respectively.

The corresponding MFs for the input variables P_G and I_{SMES} are shown in Figs. 6 and 7, respectively. The MFs for the output variable (duty cycle) are considered on the scale of 0 to 1, as shown in Fig. 8.

Center of gravity, which is widely used in fuzzy models, is used for the defuzzification process, where the desired output z_0 is calculated as [38]

$$z_0 = \frac{\int z.\mu_c(z)dz}{\int \mu_c(z)dz} \qquad (4)$$

where $\mu_c(z)$ is the MF of the output.

The variation range in the SMES current and DFIG output power, as well as the corresponding duty cycle, is used to de-velop a set of fuzzy logic rules in the form of (IF–AND–THEN)
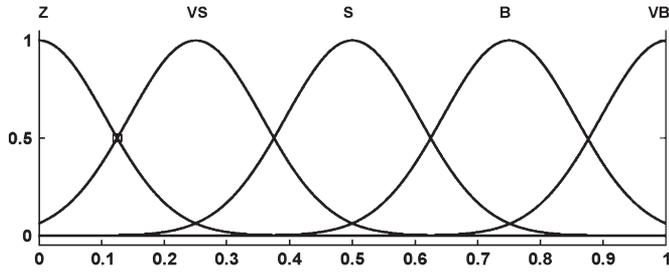
This article has been accepted for inclusion in a future issue of this journal. Content is final as presented, with the exception of pagination.

YUNUS *et al.*: APPLICATION OF SMES TO ENHANCE PERFORMANCE OF DFIG DURING VOLTAGE SAG AND SWELL 5

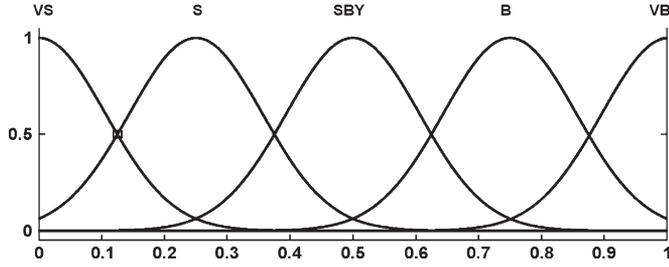Fig. 7. MF for the input variable I_{SMES} (pu).

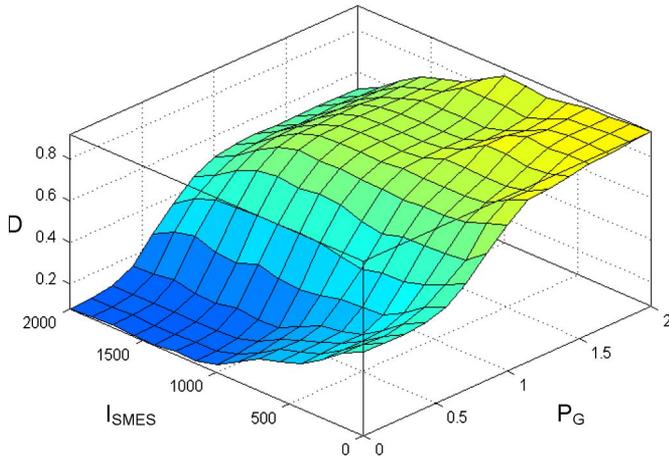Fig. 8. MF for the output variable D (duty cycle).

Fig. 9. Surface graph: duty cycle.

statements to relate the input variables to the output. The duty cycle for any set of input variable (P_G and I_{SMES}) can also be evaluated from the surface graph shown in Fig. 9.

V. SIMULATION RESULTS AND DISCUSSION

A. Voltage Sag Event

A voltage sag depth of 0.5 pu lasting for 0.05 s is applied at $t = 2$ s at the grid side of the system under study [Fig. 2(a)]. Without the SMES unit, the real power produced by the DFIG will drop to 0.6 pu, and it reaches a maximum overshooting of 40% during the clearance of the fault, as shown in Fig 10(a). As can be seen in Fig 10(a), with the SMES unit connected to the system, the DFIG output power will drop to only 0.875 pu. Fig. 10(b) implies that, with the connection of the SMES unit and during the event of voltage sag, the reactive power support by the DFIG is reduced, and the steady-state condition is reached faster, compared to the system without
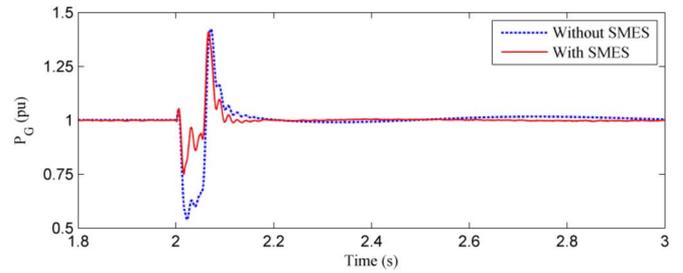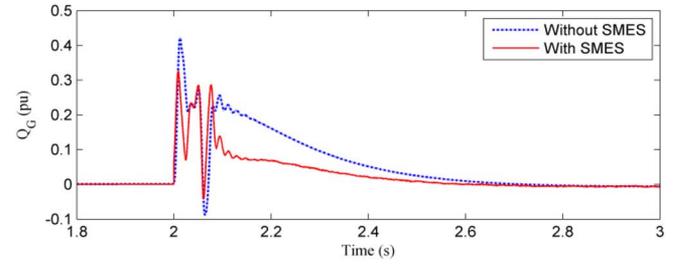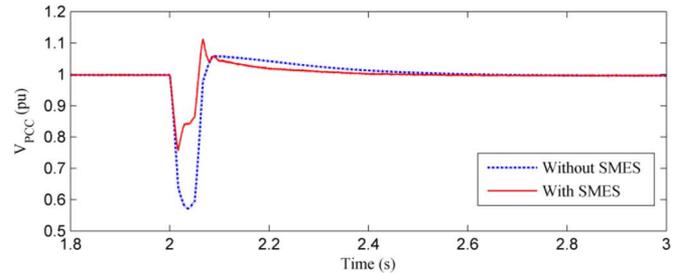
Fig. 10. DFIG responses during voltage sag without/with an SMES unit. (a) Active power. (b) Reactive power. (c) PCC voltage. (d) Shaft speed. (e) Voltage at the dc-link of the DFIG.

SMES. The voltage at the PCC is shown in Fig. 10(c), where without SMES, voltage will drop to 0.6 pu. However, by connecting the SMES unit, voltage drop at the PCC will be reduced to only 0.8 pu, which will lead to a voltage drop at the generator terminal to a level of 0.8 pu, which is referenced

This article has been accepted for inclusion in a future issue of this journal. Content is final as presented, with the exception of pagination.

6

IEEE TRANSACTIONS ON APPLIED SUPERCONDUCTIVITY

as a safety margin by the wind turbine manufacturers [39]. The DFIG power drop causes the generator speed to be accelerated to compensate for the power imbalance. As can be observed in Fig. 10(d), the generator speed will accelerate and oscillate without the SMES unit; however, with the SMES connected to the system, the power drop is reduced, the settling time of the generator speed is substantially reduced, and the overshooting level is significantly decreased. Another effect of the voltage sag on the DFIG's behavior is on the voltage across the DFIG dc link capacitor that is shown in Fig. 10(e). The voltage overshoot across the dc-link capacitor during fault clearance is slightly reduced with the SMES unit connected to the system.

B. Voltage Swell Event

Voltage swell can occur due to switching off a large load or switching on a large capacitor bank. In this simulation, a voltage swell is applied by increasing the voltage level at the grid side to 1.5 pu. The voltage swell is assumed to start at $t = 2$ s and lasts for 0.05 s. In this event, the DFIG-generated power will increase upon the swell occurrence and will be reduced when it is cleared, as shown in Fig. 11(a).

The maximum power overshoot is slightly reduced with the SMES unit connected to the system. To compensate for the voltage rise, DFIG will absorb the surplus reactive power, as shown in Fig. 11(b). The amount of reactive power absorbed by the DFIG is lesser with SMES connected to the PCC since the voltage profile at the PCC is rectified to a level below 1.3 pu with the connection of the SMES unit, whereas this voltage will remain above 1.3 pu without SMES connected to the PCC [Fig. 11(c)]. Without the connection of the SMES unit, the voltage at the PCC does not comply with the high voltage ride through (HVRT) of Spain and Australia grid codes [13], [14], which will lead to the disconnection of the DFIG from the system. The shaft speed [shown in Fig. 11(d)] is slightly improved with the connection of the SMES unit to the system. Without the connection of the SMES unit, the voltage across the DFIG dc-link capacitor will experience significant oscillations and overshooting level upon voltage swell incidence, as can be shown in Fig. 11(e). In some occasions, this may lead to the blocking of the converters [39]. As shown in Fig. 11(e), voltage oscillations, as well as voltage overshooting level, are significantly reduced by connecting the SMES unit to the system.

C. SMES Responses during Voltage Sag and Swell

The current I_{SMES} passing through the superconducting inductor is unidirectional; however, the voltage V_{SMES} across the inductor terminals can be varied in a wide range between positive and negative values through the control of the duty cycle of the dc–dc chopper (D); thus, reversibility, as well as magnitude control of power flow, is achieved continuously and smoothly through the control of the duty cycle. There are three operation modes of the SMES unit.

1) Standby mode occurs when D is equal to 0.5. The voltage across the SMES coil is equal to zero, and the SMES coil current is held constant at its rated value (2 kA for the
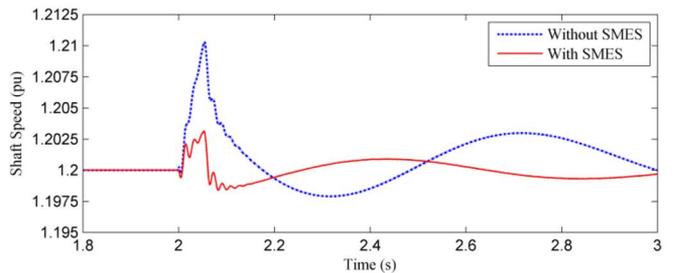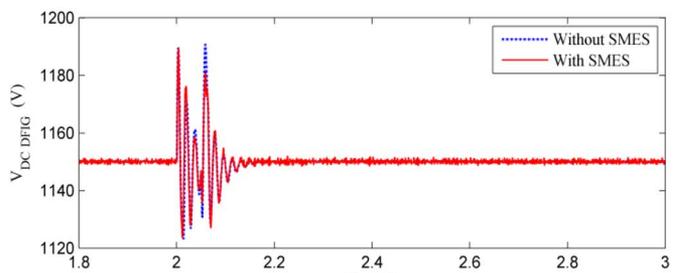

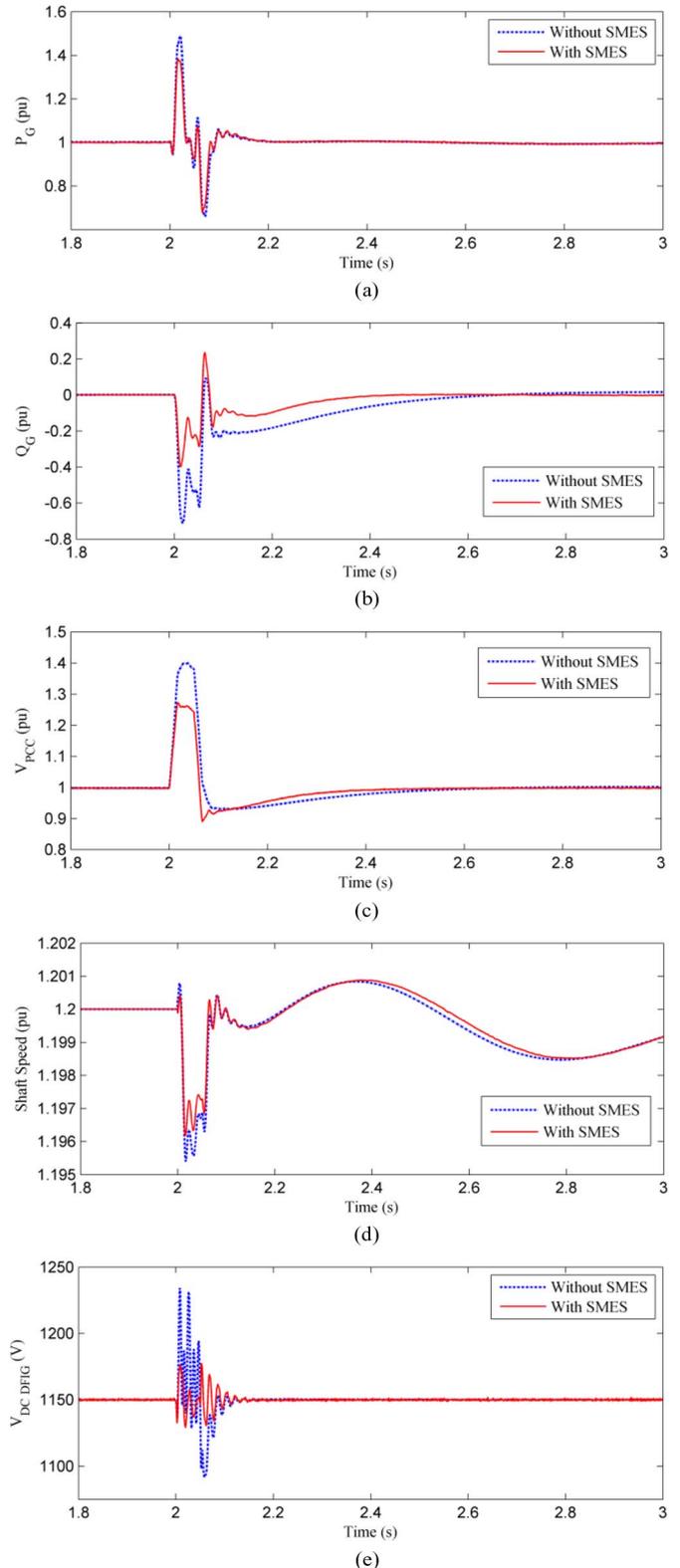Fig. 11. DFIG responses during voltage swell without/with an SMES unit. (a) Active power. (b) Reactive power. (c) PCC voltage. (d) Shaft speed. (e) Voltage at the dc-link of the DFIG.

SMES unit under study); consequently, there will be no energy transferred between the SMES unit and the AC system, and maximum energy (1 MJ for the SMES unit under study) is stored within the superconductor coil. The

This article has been accepted for inclusion in a future issue of this journal. Content is final as presented, with the exception of pagination.

YUNUS *et al.*: APPLICATION OF SMES TO ENHANCE PERFORMANCE OF DFIG DURING VOLTAGE SAG AND SWELL   7
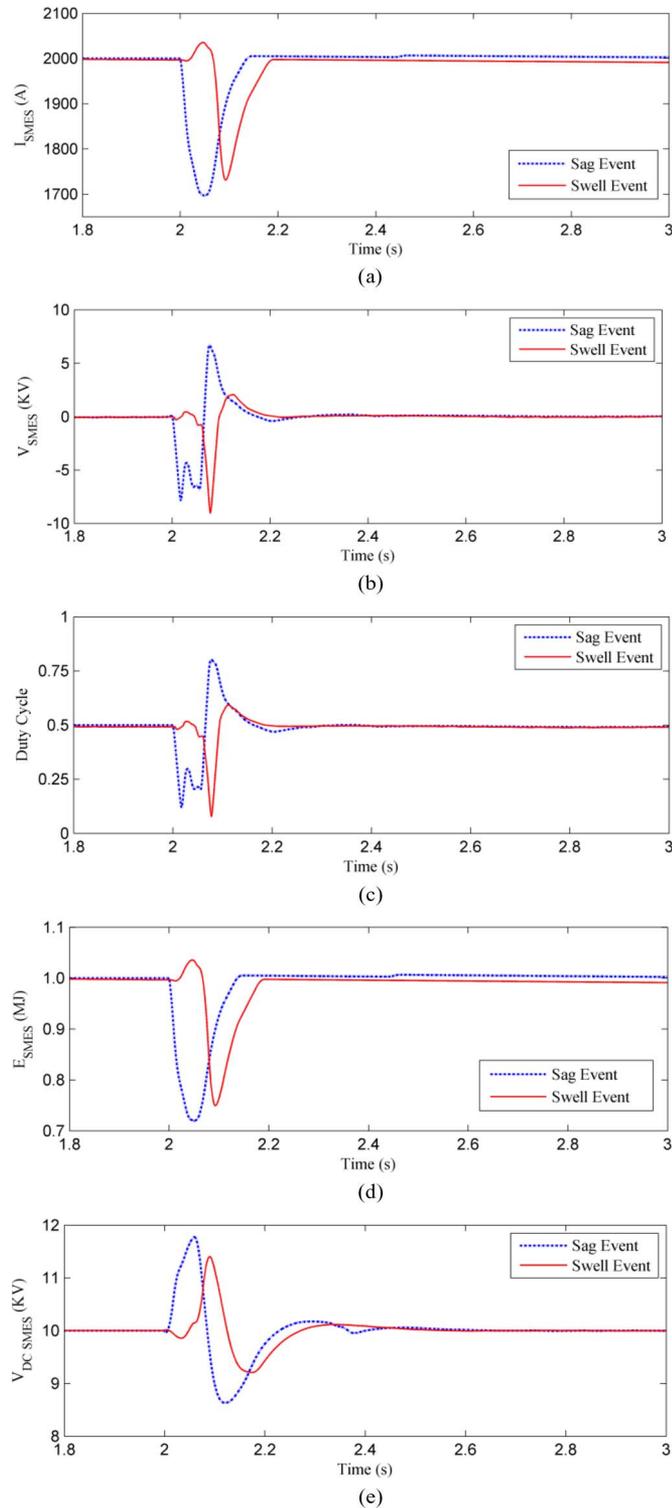

Fig. 12.   SMES transient responses during voltage sag and swell including (a) stored energy, (b) current, (c) voltage, (d) duty cycle, and (e) voltage at the dc-link of the SMES.

voltage across the dc-link capacitor of the SMES configuration ($V_{DC,SMES}$) is maintained at a constant level of 10 kV during this mode of operation. This mode will take place during normal operating condition of the WECS and is shown in Fig. 12 prior and after the occurrence of the fault.

2) Discharging mode will take place when voltage sag disturbance occurs at the grid side. In this case, the value of D lies in the range of 0–0.5. When voltage sag occurs at $t = 2$ s, the SMES coil current decreases, giving a negative slope (di/dt), and consequently, the voltage across the coil is turning negative. The magnitude of the voltage across the SMES coil is controlled by the level of the duty cycle, as well as the voltage across the SMES dc-link capacitor as given in (2). The energy stored in the coil is being delivered to the AC system during this mode, and the coil will be recharged at $t = 2.05$ s, exactly at the time when the fault is cleared according to the rules of the designated FLC for P_G and I_{SMES}. During discharging mode, the rate of coil current change is decided by the level of the duty cycle. It is observed that the SMES voltage V_{SMES} responds rapidly, and the transfer of SMES energy is done immediately upon the occurrence of voltage sag at $t = 2$ s. This mode of operation is shown by the dashed plots in Fig. 12 during the period $t = 2$ s to $t = 2.2$ s.

3) Charging mode will take place when voltage swell disturbance occurs at the grid side. In this case, the value of D lies in the range of 0.5–1. When voltage swell occurs at $t = 2$ s, the SMES coil current increases, giving a positive slope (di/dt), and consequently, the voltage across the coil is turning positive. The energy is transferred from the system to the SMES coil until the maximum coil energy capacity designated by the fuzzy rules is reached (1.03 MJ in the system under study to allow for power modulation during voltage swell disturbance) after which the voltage across the SMES coil decreases and returns back to zero level when the maximum current in the SMES coil is reached. This mode of operation is shown by the solid plots in Fig. 12 during the period $t = 2$ s to $t = 2.2$ s.

The following general observations can be concluded.

It can be observed that the SMES coil current in both voltage sag and voltage swell events has a similar trend to the coil stored energy and their levels at any time are mathematically correlated by the relation given in (1).

In both voltage sag and voltage swell events, voltage across the SMES coil will be maintained at zero level once the maximum current in the SMES coil is reached. Once a system with SMES unit has regained post fault stability, the SMES coil is not preferred to be kept on continuously to avoid the draining process of SMES energy during normal operating conditions. Furthermore, turning it off can reduce the generator shaft speed oscillations to some extent. It also reduces the operating expenses of the SMES unit. This is achieved by short circuiting the SMES coil through a bypass switch shown in Fig. 5(a).

In both the voltage sag and voltage swell events, it is observed that the voltage across the dc-link capacitor of the SMES configuration ($V_{DC,SMES}$) oscillates in an opposite manner to V_{SMES}, and its level at any time is related to the level of V_{SMES}. The level of V_{SMES} at any time is correlated to the level of $V_{DC,SMES}$ and the duty cycle value by the relation given in (2).

This article has been accepted for inclusion in a future issue of this journal. Content is final as presented, with the exception of pagination.

8   IEEE TRANSACTIONS ON APPLIED SUPERCONDUCTIVITY

TABLE IV
PARAMETERS OF THE SMES UNIT

Rated Energy	1.0 MJ
L_{SMES}	0.5 H
I_{SMES}	2000 A

The maximum voltage overshoot in $V_{DC,SMES}$ shown in Fig. 12(d) still remains within a safety margin of 1.25 pu of the nominal value [39], which corresponds to 12 kV in the studied case. It is also noted that the voltage across the SMES coil and the duty cycle have the same trend during the disturbance event. This aligns well with the results presented in [31].

D. SMES Capacity

The SMES unit capacity depends on the application and charging/discharging duration. Very high energy rating has excellent impact on damping oscillations rapidly, but the cost of the unit will be too high due to large current in the coil. Meanwhile, if the energy rating is too low, the output of the SMES unit will be limited during disturbances, and it will not be very effective in controlling system oscillations quickly. The first SMES unit rated 30 MJ with a rated coil current of 5 kA was installed in Bonneville power administration, Tacoma, in 1982 [40]. An SMES coil energy E_{SMES} of value less than 0.15 of the generator rated power will be adequate in safeguarding against momentary power interruption [17], [18]. In the system under study, the DFIG rated power is 9 MW, and the rated energy of the SMES coil is designed to be 1 MJ. As the SMES coil inductance is chosen to be 0.5 H, the inductor nominal current is 2 kA (Table IV). To make the SMES coil effective in voltage swell events, the rated inductor current is set at a level higher than the nominal coil current [41]. In the system under study, the rated coil current was chosen to be 2.03 kA. This will allow the SMES coil to absorb maximum energy up to 1.03 MJ during the voltage swell event.

VI. CONCLUSION

A new control algorithm along with a new application of the SMES unit to improve the transient response of WTGs equipped with DIFG during voltage sag and voltage swell events has been proposed. Simulation results have shown that the SMES unit is very effective in improving the dynamic performance of a power system with wind turbine equipped with DFIG during voltage sag and voltage swell at the grid side. The proposed control algorithm of the SMES unit is simple and easy to implement and is able to improve the FRT of the DFIG. The SMES unit, on the other hand is still a costly piece of equipment; however, due to the development of high-temperature superconducting materials, its application in power systems is expected to become viable in the near future.

ACKNOWLEDGMENT

REFERENCES

[1] L. Freris and D. Infield, *Renewable Energy in Power Systems*. Wiltshire, U.K.: Wiley, 2008, p. 217.

[2] P. Musgrove, *Wind Power*. New York: Cambridge Univ. Press, 2010, pp. 221–222.

[3] J. M. Carrasco, L. G. Franquelo, J. T. Bialasiewicz, E. Galvan, R. C. P. Guisado, M. A. M. Prats, J. I. Leon, and N. Moreno-Alfonso, "Power-electronic systems for the grid integration of renewable energy sources: A survey," *IEEE Trans. Ind. Electron.*, vol. 53, no. 4, pp. 1002–1016, Jun. 2006.

[4] T. Ackerman, *Wind Power in Power System*. West Sussex, U.K.: Wiley, 2005, p. 65.

[5] M. Tsili and S. Papathanassiou, "A review of grid code technical requirements for wind farms," *IET Renew. Power Gener.*, vol. 3, no. 3, pp. 308–332, Sep. 2009.

[6] S. Seman, J. Niiranen, and A. Arkkio, "Ride-through analysis of doubly fed induction wind-power generator under unsymmetrical network disturbance," *IEEE Trans. Power Syst.*, vol. 21, no. 4, pp. 1782–1789, Nov. 2006.

[7] J. Lopez, E. Gubia, E. Olea, J. Ruiz, and L. Marroyo, "Ride through of wind turbines with doubly fed induction generator under symmetrical voltage dips," *IEEE Trans. Ind. Electron.*, vol. 56, no. 10, pp. 4246–4254, Oct. 2009.

[8] M. Mohseni, S. M. Islam, and M. A. S. Masoum, "Impacts of symmetrical and asymmetrical voltage sags on DFIG-based wind turbines considering phase-angle jump, voltage recovery, and sag parameters," *IEEE Trans. Power Electron.*, vol. 26, no. 5, pp. 1587–1598, May 2011.

[9] Y. Xiangwu, G. Venkataramanan, P. S. Flannery, W. Yang, D. Qing, and Z. Bo, "Voltage-sag tolerance of DFIG wind turbine with a series grid side passive-impedance network," *IEEE Trans. Energy Convers.*, vol. 25, no. 4, pp. 1048–1056, Dec. 2010.

[10] S. Hu, X. Lin, Y. Kang, and X. Zou, "An improved low-voltage ride-through control strategy of doubly fed induction generator during grid faults," *IEEE Trans. Power Electron.*, vol. 26, no. 12, pp. 3653–3665, Dec. 2011.

[11] J. G. Slootweg, S. W. H. de Haan, H. Polinder, and W. L. Kling, "General model for representing variable speed wind turbines in power system dynamics simulations," *IEEE Trans. Power Syst.*, vol. 18, no. 1, pp. 144–151, Feb. 2003.

[12] F. Blaabjerg and Z. Chen, *Power Electronics for Modern Wind Turbines*. Aalborg, Denmark: Morgan & Claypool, 2006, p. 18.

[13] M. Altin, O. Goksu, R. Teodorescu, P. Rodriguez, B. B. Jensen, and L. Helle, "Overview of recent grid codes for wind power integration," in *Proc. 12th Int. Conf. OPTIM*, 2010, pp. 1152–1160.

[14] AEMO. [Online]. Available: www.aemo.com.au

[15] H. J. Boenig and J. F. Hauer, "Commissioning tests of the bonneville power administration 30 MJ superconducting magnetic energy storage unit," *IEEE Trans. Power App. Syst.*, vol. PAS-104, no. 2, pp. 302–312, Feb. 1985.

[16] M. H. Ali, W. Bin, and R. A. Dougal, "An overview of SMES applications in power and energy systems," *IEEE Trans. Sustainable Energy*, vol. 1, no. 1, pp. 38–47, Apr. 2010.

[17] A. Abu-Siada, "Application of superconducting magnetic energy storage units to improve power system performance," Ph.D. thesis, Dept. Elect. Eng., Curtin Univ. Technol., Bentley, Australia, 2004.

[18] A. Abu-Siada and S. Islam, "Application of SMES unit in improving the performance of an AC/DC power system," *IEEE Trans. Sustainable Energy*, vol. 2, no. 2, pp. 109–121, Apr. 2011.

[19] J. Hee-Yeol, A. R. Kim, K. Jae-Ho, P. Minwon, Y. In-Keun, K. Seok-Ho, S. Kideok, K. Hae-Jong, S. Ki-Chul, T. Asao, and J. Tamura, "A study on the operating characteristics of SMES for the dispersed power generation system," *IEEE Trans. Appl. Supercond.*, vol. 19, no. 3, pp. 2028–2031, Jun. 2009.

[20] S. S. Chen, L. Wang, W. J. Lee, and Z. Chen, "Power flow control and damping enhancement of a large wind farm using a superconducting magnetic energy storage unit," *IET Renew. Power Gener.*, vol. 3, no. 1, pp. 23–38, Mar. 2009.

[21] M. H. Ali, P. Minwon, Y. In-Keun, T. Murata, and J. Tamura, "Improvement of wind-generator stability by fuzzy-logic-controlled SMES," *IEEE Trans. Ind. Appl.*, vol. 45, no. 3, pp. 1045–1051, May/Jun. 2009.

[22] F. Zhou, G. Joos, C. Abbey, L. Jiao, and B. T. Ooi, "Use of large capacity SMES to improve the power quality and stability of wind farms," in *Proc. IEEE Power Eng. Soc. Gen. Meeting*, 2004, vol. 2, pp. 2025–2030.

This article has been accepted for inclusion in a future issue of this journal. Content is final as presented, with the exception of pagination.

YUNUS *et al.*: APPLICATION OF SMES TO ENHANCE PERFORMANCE OF DFIG DURING VOLTAGE SAG AND SWELL

9

[23] M. R. I. Sheikh, S. M. Muyeen, R. Takahashi, T. Murata, and J. Tamura, "Minimization of fluctuations of output power and terminal voltage of wind generator by using STATCOM/SMES," in *Proc. IEEE Bucharest PowerTech*, 2009, pp. 1–6.

[24] T. Asao, R. Takahashi, T. Murata, J. Tamura, M. Kubo, A. Kuwayama, and T. Matsumoto, "Smoothing control of wind power generator output by superconducting magnetic energy storage system," in *Proc. ICEMS*, 2007, pp. 302–307.

[25] J. Hee-yeol, P. Dae-Jin, S. Hyo-Ryong, P. Minwon, and Y. In-Keun, "Power quality enhancement of grid-connected wind power generation system by SMES," in *Proc. IEEE/PES PSCE*, 2009, pp. 1–6.

[26] W. Li, C. Shiang-Shong, L. Wei-Jen, and C. Zhe, "Design of a damping controller for a SMES unit to suppress tie-line active-power fluctuations of a large-scale wind farm," in *Proc. IEEE/PES PSCE*, 2009, pp. 1–7.

[27] P. F. Ribeiro, B. K. Johnson, M. L. Crow, A. Arsoy, and Y. Liu, "Energy storage systems for advanced power applications," *Proc. IEEE*, vol. 89, no. 12, pp. 1744–1756, Dec. 2001.

[28] S. C. Smith, P. K. Sen, and B. Kroposki, "Advancement of energy storage devices and applications in electrical power system," in *Proc. IEEE Power Energy Soc. Gen. Meeting—Convers. Del. Elect. Energy 21st Century*, 2008, pp. 1–8.

[29] H. Chen, T. N. Cong, W. Yang, C. Tan, Y. Li, and Y. Ding, "Progress in electrical energy storage system: A critical review," *Progr. Natural Sci.*, vol. 19, no. 3, pp. 291–312, Mar. 2009.

[30] E. Ancha, V. G. Agelidis, O. Anaya-Lara, and T. J. E. Miller, *Power Electronic Control in Electrical Systems*. Oxford, U.K.: Newnes, 2002.

[31] I. D. Hassan, R. M. Bucci, and K. T. Swe, "400 MW SMES power conditioning system development and simulation," *IEEE Trans. Power Electron.*, vol. 8, no. 3, pp. 237–249, Jul. 1993.

[32] A. R. Kim, S. Hyo-Ryong, K. Gyeong-Hun, P. Minwon, Y. In-Keun, Y. Otsuki, J. Tamura, K. Seok-Ho, S. Kideok, and S. Ki-Chul, "Operating characteristic analysis of HTS SMES for frequency stabilization of dispersed power generation system," *IEEE Trans. Appl. Supercond.*, vol. 20, no. 3, pp. 1334–1338, Jun. 2010.

[33] S. Jing, T. Yuejin, X. Yajun, R. Li, and L. Jingdong, "SMES based excitation system for doubly-fed induction generator in wind power application," *IEEE Trans. Appl. Supercond.*, vol. 21, no. 3, pp. 1105–1108, Jun. 2011.

[34] M. G. Molina and P. E. Mercado, "Power flow stabilization and control of microgrid with wind generation by superconducting magnetic energy storage," *IEEE Trans. Power Electron.*, vol. 26, no. 3, pp. 910–922, Mar. 2011.

[35] K. Bong-Hwan, K. Tae-Woo, and Y. Jang-Hyoun, "A novel SVM-based hysteresis current controller," *IEEE Trans. Power Electron.*, vol. 13, no. 2, pp. 297–307, Mar. 1998.

[36] M. Milosevic, *Hysteresis Current Control in Three-Phase Voltage Source Inverter*, Feb. 19, 2011. [Online]. Available: http://www.eeh.ee.ethz.ch/uploads/tx_ethpublications/milosevic_hysteresis.pdf

[37] L. Malesani and P. Tenti, "A novel hysteresis control method for current-controlled voltage-source PWM inverters with constant modulation frequency," *IEEE Trans. Ind. Appl.*, vol. 26, no. 1, pp. 88–92, Jan./Feb. 1990.

[38] H. Li and M. M. Gupta, *Fuzzy Logic and Inteligent System*. Norwell, MA: Kluwer, 1995.

[39] V. Ahkmatov, "Analysis of dynamic behaviour of power systems with large amount of wind power," Ph.D. thesis, Tech. Univ. Denmark, Lyngby, Denmark, Feb. 25, 2011.

[40] J. Rogers, H. Boenig, R. Schermer, and J. Hauer, "Operation of the 30 MJ superconducting magnetic energy storage system in the Bonneville Power Administration electrical grid," *IEEE Trans. Magn.*, vol. MAG-21, no. 2, pp. 752–755, Mar. 1985.

[41] M. G. Rabbani, J. B. X. Devotta, and S. Elangovan, "Application of simultaneous active and reactive power modulation of SMES unit under unequal α-mode for power system stabilization," *IEEE Trans. Power Syst.*, vol. 14, no. 2, pp. 547–552, May 1999.

A. M. Shiddiq Yunus (S'11) was born in Makassar, Indonesia. He received the B.Sc. degree in electrical engineering from Hasanuddin University, Makassar, Indonesia, in 2000 and the M.Eng.Sc. degree in electrical engineering from Queensland University of Technology, Brisbane, Australia, in 2006. He is recently working toward the Ph.D. degree at Curtin University, Perth, Australia.

He has been a Lecturer with the Department of Mechanical Engineering, Energy Conversion Study Program, State Polytechnic of Ujung Pandang, Makassar, Indonesia, since 2001. His research interests include superconducting magnetic energy storage, renewable energy, and smart grids.

Mohammad A. S. Masoum (S'88–M'91–SM'05) received the B.S., M.S., and Ph.D. degrees in electrical and computer engineering from the University of Colorado, Denver, in 1983, 1985, and 1991, respectively.

He is currently an Associate Professor and the Discipline Leader and Course Coordinator for Power System Engineering with the Department of Electrical and Computer Engineering, Curtin University, Perth, Australia. He is a coauthor of *Power Quality in Power Systems and Electrical Machines* (Elsevier, 2008) and *Power Conversion of Renewable Energy Systems* (Springer, 2011). His research interests include optimization, power quality and stability of power systems/electric machines, and distributed generation.

A. Abu-Siada (M'07) received the B.Sc. and M.Sc. degrees in electrical engineering from Ain Shams University, Cairo, Egypt, and the Ph.D. degree in electrical engineering from Curtin University, Perth, Australia.

He is currently a Lecturer with the Department of Electrical and Computer Engineering, Curtin University. His research interests include power system stability, condition monitoring, superconducting magnetic energy storage, power electronics, power quality, energy technology, and system simulation.

Dr. Abu-Siada is a Regular Reviewer for the IEEE Transactions on Power Electronics, IEEE Transaction on Power Delivery, and IEEE Transactions on Dielectrics and Electrical Insulation.